A benzoxazine/substituted borazine composite coating: A new resin for improving the corrosion resistance of the pristine benzoxazine coating applied on aluminum

Alexis Renaud[a], Leïla Bonnaud[b], Ludovic Dumas[b], Tao Zhang[b], Yoann Paint[c], Francesco Fasano[d], Olesia Kulyk[d], Eva Pospisilova[e], Bernard Nysten[e], Arnaud Delcorte[e], Davide Bonifazi[d], Philippe Dubois[b], Marie-Georges Olivier[a], Marc Poorteman[a]

[a] *Department of Materials Science, Materials Engineering Research Center (CRIM), University of Mons, Place du Parc 20, B-7000 Mons, Belgium*

[b] *Laboratory of Polymeric and Composite Materials, Center of Innovation and Research in Materials and Polymers (CIRMAP), Materia Nova Research Center & University of Mons, Place du Parc 20, B-7000 Mons, Belgium*

[c] *Materia Nova Asbl, Avenue Copernic 1, B-7000 Mons, Belgium*

[d] *School of Chemistry, Cardiff University, Park Place Main Building, Cardiff CF10 3AT, United Kingdom*

[e] *Université Catholique de Louvain, Institute of Condensed Matter and Nanoscience, 1 Place Louis Pasteur, B-1348 Louvain-la-Neuve, Belgium*

ARTICLE INFO

Keywords:
Benzoxazine coating
Borazine derivative
Composite resin, Thermal curing
Barrier properties
Electrochemical Impedance Spectroscopy

ABSTRACT

In this paper, laboratory synthesized Phenol-paraPhenyleneDiAmine (P-pPDA) benzoxazine containing different amounts of B-trimesityl-N-triphenylborazine was applied by spin coating on aluminum and thermally cured. The addition of the borazine derivative (borazine **1**) does not appear to modify the curing characteristics of the P-pPDA matrix itself as shown by FTIR, DSC and DEA analyses; however, some interactions - chemical and/or physical (co-crystallization) – between P-pPDA and borazine **1** cannot be excluded. The microstructure of the composites is character-ized by a two phase system consisting of a dispersion of nanosized (10–20nm) clusters for the lowest borazine **1** concentration (0.5wt%), evolving towards bigger (100–200nm), agglomerated clusters for higher borazine **1** concentrations (3wt%) and finally, continuous, dendritic structures within the P-pPDA matrix for the highest borazine **1** concentration (10wt%). The benzoxazine composite coating containing 0.5wt% trimesitylborazine derivative showed a largely increased and durable ability to protect the aluminum substrate. It is shown that a highly capacitive be-havior and durable barrier properties can be obtained for P-pPDA coatings containing such a low amount of borazine derivative homogeneously dispersed in the benzoxazine matrix. For concen-trations of 3wt%, as agglomeration took place and dendrites appeared for the highest concentra-tion of borazine derivative (10wt%), the corrosion resistance decreased with time.

1. Introduction

Metals and their alloys are materials widely used in many fields as structural components. However, when used in infrastructures and aeronautic applications, they are exposed to outside environments and, depending on the severity of the conditions, start to corrode after a given time. Therefore, they have to be protected from the outside and this can be achieved by the application of a protective coating on the metal, acting as a physical barrier and limiting the access of aggressive species to the metal surface.

Email address: marc.poorteman@umons.ac.be (M. Poorteman)

More specifically, in the aircraft industry, lightweight materials are preferentially used to lower the energy cost of air transport and, therefore, aluminum is largely preferred for metallic structural components. However, the mechanical properties of aluminum are too low for bearing the mechanical stresses to be supported during flights and therefore, aluminum alloys with improved mechan-ical properties have been developed.

Alloys from series 2xxx and 7xxx, containing significant amounts of Cu and Zn/Mg respectively, are the most used in the aircraft industry due to their highly improved mechanical properties. In particular, the aluminum alloy 2024 is massively employed in fuse-lage and skin pieces where high toughness, mechanical strength and fatigue resistance are required. In order to maximize its mechan-ical performance, the usual thermo-mechanical process applied to this alloy, is a common temper T3, corresponding to a solution heat treatment followed by a cold working and a final natural aging. As a member from the 2xxx group, the AA2024-T3 contains copper as main alloying element (between 3.8 and 4.9wt%). The thermomechanical precipitation hardening process gives a particular het-erogeneous microstructure to the material, and several kinds of copper containing intermetallic precipitates can be observed, which are responsible for the high corrosion sensitivity of AA2024-T3 alloys.

To ensure the security in the aircraft and to limit the costs of maintenance, the surface of aluminum pieces has to be protected from corrosion. In order to improve its corrosion protection, AA2024-T3 substrates can also be used with a clad deposit of AA1050 alloy (mainly pure aluminum) on top of its surface. For further improving the corrosion protection, a wide range of organic coatings has been developed and applied onto aluminum based substrates providing a passive and/or active corrosion protection. Up to now, epoxy resins are the most commonly used thermoset polymers for such kind of applications [1,2].

Polybenzoxazine resins have been reported in the literature to show several remarkable properties such as low water uptake, a high thermal stability, low shrinkage during curing [3] as well as a low dielectric constant [4]. These characteristics make them very suitable for coating protection applications [5,6]. Benzoxazine monomers are obtained by simple condensation of formaldehyde, a phenol group and a primary amine, conferring a wide versatility to benzoxazine monomer compositions [7–10]. However, in the selection of the coating to be applied, care has to be taken as some of these resins have been reported to suffer from drawbacks. Indeed, in the case of bisphenol-based benzoxazine, an irreversible degradation process, accompanied with the release of volatile imino species [11], occurs during thermal curing causing the occurrence of defects within the polymer (bubbles, cracks) compromis-ing the barrier properties and therefore the reliability of the coating. Such defects can be avoided by selecting a more appropriate molecular design. Indeed, phenol-para-phenylenediamine based benzoxazine monomers (P-pPDA) have been recently reported in the literature [6,9,10] showing a higher thermal stability during curing leading to coatings with promising barrier properties. However, when P-pPDA coatings are applied on bare AA1050, after several days of immersion in a NaCl solution, delamination processes at the metal/coating interface have been reported in the literature, leading to a loss of corrosion protection [6] again compromising the reliability of the barrier coating.

In the case of epoxy coatings applied on steel, a recent paper has reported delamination also to occur during the same kind of immersion tests leading to a decrease of corrosion resistance for long times of immersion, reducing the durability of the coating [12,13]. Addition of well dispersed h-BN nanoplatelets in small concentrations – 0.5 to 1wt% - in the epoxy matrix appeared to strongly increase the corrosion resistance of the composite making the coating durable. In order to obtain a homogeneous dispersion of the nanoplatelets in the polymer matrix, amine capped aniline trimer (AT) was added as a dispersant. Composites with higher concentrations started to agglomerate starting from 2wt% h-BN, which can be attributed to the high aspect ratio of the platelets. Indeed, percolation theory [14] describes the evolution of the organization of isotropic spheres in an isotropic matrix as follows: first, the spheres are homogeneously dispersed in the matrix. For higher concentration, discontinuous clustering occurs, corresponding to the formation of aggregates. Finally starting from 18vol.%, the spheres are percolating forming continuous clusters throughout the matrix. The concentration for discontinuous clustering and percolation is lowered when the particles are anisotropic such as 2D struc-tures – platelets – and 1D structures – fibers. For instance, when carbon nanotubes are dispersed in a benzoxazine matrix, percolation occurs at concentrations as low as 0.3wt% [9,15–17]. Due to this agglomeration, defects are created increasing the porosity of the polymer and, consequently, leading to a decrease of the polarization resistance and therefore reduced corrosion resistance.

A homogeneous dispersion of h-BN in a polymer matrix such as epoxy without agglomerates is a necessary but insufficient condi-tion to increase the corrosion resistance of the coating in a durable way. Indeed, h-BN has a 2-D structure analogous to graphene. It has been reported in the literature that h-BN, just as graphene, because of its high impermeability, is acting as a corrosion barrier able to protect metallic surfaces from corroding [18]. However, when graphene or h-BN monolayers are deposited on a copper substrate, though the corrosion resistance of both is excellent for short times of exposure to corrosive liquid media, the long-term barrier prop-erties of the graphene layer are compromised, whereas the h-BN layer maintains its properties. This has been attributed to the high electrical conductivity of the graphene, at the opposite of h-BN, which is insulating, suppressing the galvanic corrosion taking place when graphene is used.

A homogeneous dispersion and the insulating properties of platelet nanoparticles, such as h-BN, appear to be promising for im-proving the barrier properties of thermoset coatings applied on metals.

In this paper, the authors propose to use an approach with the aim of satisfying the previously mentioned conditions in order to improve the barrier properties of a cured P-pPDA coating applied on bare aluminum (AA1050). Instead of using h-BN nanoplatelets, the borazine **1** derivative (Bz**1**), bearing mesityl groups at the boron centers, was exploited (Fig. 1b).

Though the design of the trimesitylborazine derivative is somewhat different compared to h-BN, borazine **1** has some characteris-tic properties in line with those of h-BN. Indeed, in the adapted molecular design, the borazine core displays an extraordinary stability towards hydrolysis, suggesting that the mesityl substituents exert a steric hindrance at the B atom centers, thus mimicking the in-ert and hydrophobic nature of h-BN. Moreover, the chosen borazine **1** is electrically insulating, as in the case of h-BN. Furthermore,

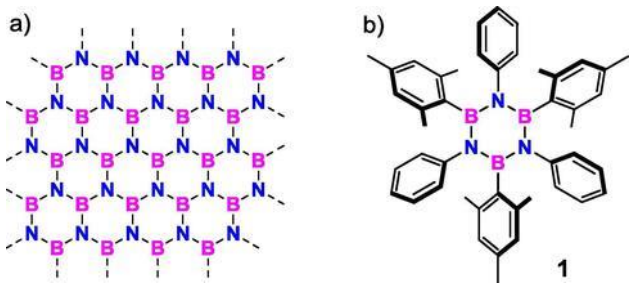

Fig. 1. (a) 2D structure of h-BN; (b) chemical structure of borazine derivative **1.**

the aromatic structure of the molecule is likely to favor chemical π-π interactions with the P-pPDA aromatic molecules [19] and, consequently, improving the dispersion of borazine **1** in the benzoxazine matrix.

Finally, the approach followed by the authors is an alternative approach for the one they have recently reported in the literature for improving the corrosion properties of P-pPDA benzoxazine applied on bare aluminum, through anodization of the aluminum substrate [20].

2. Experimental part

2.1. Materials

For the synthesis of P-pPDA, the following chemicals were purchased from Aldrich and used without further purification: 1,4-phenylenediamine (99%), phenol (99%) and paraformaldehyde (95%). Technical chloroform was purchased from *VWR* and used as received.

For the synthesis of B-trimesityl-N-triphenylborazine, aniline (99%), BCl_3 (1M solution in toluene), 2-bromomesitylene (98%), *n*-BuLi (1.36M in hexane) were purchase from *Sigma Aldrich* and used without further purification·THF and toluene were dried on a Braun MB SPS-800 solvent purification system and further kept over activated 4Å molecular sieves. EtOAc and cyclohexane were purchased from *Fisher Chemical* and used as received. B-trimesityl-N-triphenylborazine **1** was synthesized in 40% yield following the previously reported protocol [21].

2.2. Preparation process of aluminum substrate and coating

2.2.1. Preparation process of the aluminum substrate

The chemical composition of the AA1050 aluminum alloy in weight percent is: <0.40%Fe, <0.25%Si, <0.07%Zn, <0.05%Cu, <0.05%Mg, <0.05%Ti, <0.05%Mn and Al accounts for the remainder.

Aluminum samples (60mm×45mm×1mm) were treated in different steps in order to enable the formation of a homogeneous oxide layer. The different steps are as follows: degreasing in acetone, etching in 1M NaOH at 40°C for 1min, desmutting in Turco® Liquid Smut-Go NC Deoxidizer at room temperature for 15s with rinsing in deionized water between each step.

*2.2.2. Synthesis of borazine **1** derivative and P-pPDA*

Following the *Brown* and *Groszos*'s synthetic protocol [22], the trimesitylborazine **1** derivative was synthesized by the *Bonifazi* group using a one-pot procedure involving BCl_3 [21] (Scheme 1). The formation of unstable B-trichloro-N-triphenylborazine **2** was followed by subsequent treatment with Li-derived reagent to afford desired B-trimesityl-N-triphenylborazine **1** in a good yield.

P-pPDA resin precursor was synthesized by a solventless synthesis from 1,4-phenylenediamine according to the reaction shown in Scheme 2 and a protocol described in a previous paper [10].

2.2.3. Coating formulation

Prior to coating, first, an organic solution of benzoxazine precursor in chloroform was prepared by dissolving 8g of P-pPDA-benzoxazine precursor in 40mL of chloroform, stirring and heating under reflux for 4h at 70°C and then cooling down to room temperature, maintaining stirring for 12h. The P-pPDA solution was then filtered using filter paper under atmospheric pressure in order to remove insoluble aggregates.

The mixing process of the synthesized borazine **1** and P-pPDA benzoxazine appeared to be very simple since the considered bo-razine is fully soluble in chloroform and can easily be mixed with the prepared P-pPDA solution leading to a homogeneous and stable solution.

Different trimesitylborazine contents in P-pPDA have been tested: 0.5, 3 and 10wt%. The corresponding composites with x wt% of trimesitylborazine are abbreviated by P-pPDA+x wt.% Bz1, except for x=0 which will be called pristine in this paper.

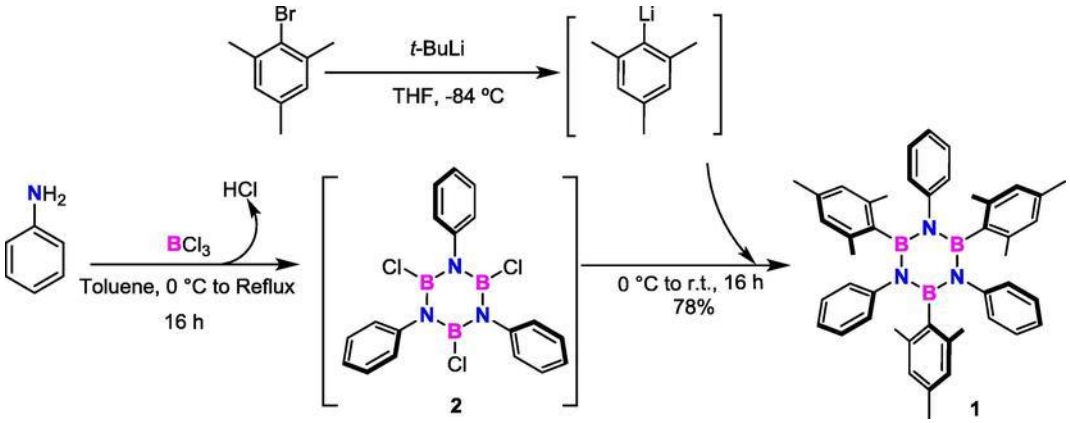

Scheme 1. Synthesis of B-trimesityl-N-triphenylborazine **1.**

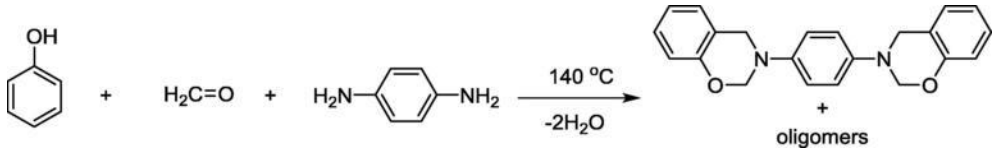

Scheme 2. One pot synthesis of P-pPDA precursor.

2.2.4. Coating process

After pretreatment of the aluminum substrates, samples were rinsed in deionized water, dried with pulsed air and directly coated with the organic solution mixture of benzoxazine precursor and borazine derivative in chloroform. This solution was applied on AA1050 substrate by deposing 1mL on the samples and spin coated at 1000rpm for 30s.

After deposition and drying of the precursor coating, thermal curing was carried out stepwise to obtain a cross-linked polymer by successive thermal curing steps: at 140°C for 60min., 180°C and 200°C, with each time a dwell of 2h, and, finally, two steps at 220°C and 230°C for 30min. each. Afterwards, samples were allowed to slowly cool down to room temperature. This curing cycle corresponds to the standard cross linking treatment of the pristine resin [6]. The samples were thermally treated in a Heraeus Instruments LUT 6050 oven in horizontal position to avoid outflow and loss of benzoxazine during the treatment.

2.3. Characterization

2.3.1. Textural, physical and chemical analysis of coated samples

The coating thicknesses were estimated by the Eddy currents method using an ELCOMETER 456 tool and by performing 20 mea-surements on different locations of the coated aluminum.

Coated samples were observed using SEM-FEG (Hitachi SU8020 with cold cathode) without metallization and coupled to an en-ergy dispersive X-ray spectrometer analyser (EDX) to investigate the elemental distribution in the observed micrographs and by AFM (Bruker Icon Dimension) using PeakForce QNM (quantitative nanomechanical property mapping) mode. Soft ScanAsyst probes with spring constant between 0.2 and 0.8N/m were used in order to obtain images of surface roughness, energy dissipation and adhe-sion. The photodetector sensitivity was calibrated using a ramping procedure on a reference sapphire sample. The cantilever spring constant was calibrated using the thermal tune procedure. An analysis was performed on the surface topography based on in-house developed routines under Igor-Pro (WaveMetrics). The chemical composition was probed by Time of Flight Secondary Ion Mass Spec-trometry (ToF-SIMS; Ion-tof GmbH) using Bi_{5+} clusters at 30keV as analysis beam for surface characterization. In the case of the interface characterization, ToF-SIMS was used in dual-beam molecular depth-profiling mode, where Ar_{1500+} at 10keV as a sputter beam erodes the material and Bi_{5+} is used to analyze the bottom of the eroded crater. The size of the crater created by the sputter beam was 450 µm×450 µm. To avoid the edge effects, the analysis crater size was 150 µm×150 µm. An automatic procedure for charge compensation was used in order to suppress the charging effect at the polymer/metal interface beam of electrons.

Static contact angles were measured on coated surfaces using a goniometer and specialized software (Digidrop –DS equipment). Two measurements, one on each side of the drop, were recorded and an average was obtained.

2.3.2. Glass transition temperature and crosslinking degree estimation of applied coatings

Calorimetric studies were carried out at a heating rate of 10°C/min. from 0 up to 315°C using a differential scanning calorimeter (DSC Q200 from TA Instruments) under nitrogen flow of 50mL/min. An Indium standard was used for calibration. The different peaks were integrated in order to estimate the enthalpy associated with the different reactions.

Fourier Transform Infrared Analysis (FTIR) measurements were carried out in the 370–2000cm^{-1} range using a Perkin Elmer Spec-trum 2000 apparatus.

For curing monitoring through DEA, a 230/2 epsilon instrument from Netzsch was used. Heating was carried out in a Heraeus Instruments LUT 6050 oven with an integrated J type thermocouple. The external interface box used was a mid-conductivity inter-face, enabling to measure electrical conductivities between 10^{-3} and 10^{-13} Scm^{-1}. An inter-digitized electrode sensor was used (IDEX 036S from Netzsch) with an electrode spacing of 130µm and an A/D ratio (cm) of 80. The thickness applied by drop casting of the benzoxazine solution on top of the sensor was largely superior to the electrode spacing. The log loss domain covered by this type of sensor is typically between 1 and 4.

2.3.3. Electrochemical properties and modeling

Electrochemical impedance measurements were performed after different immersion times in 0.1M NaCl solution on the different systems in order to characterize the evolution of their barrier properties. A conventional three-electrode cell was used for the electro-chemical tests. The working electrode was the investigated sample (exposed area of 7.07cm^2), the counter electrode was a platinum plate and all potentials were measured with respect to an Ag/AgCl/Satured KCl (+0.197V vs SHE) reference electrode. The cell was placed in a Faraday cage in order to minimize external electromagnetic interference on the system. The impedance measurements were carried out over frequencies ranging from 100kHz to 10mHz, at ambient temperature. The impedance spectra were acquired by using a potentiostat coupled with a frequency response analyser (Parstat 2273 from Ametek), computer-controlled with Powersuite® software. The signal amplitude was 30mVrms. Impedance measured data have been fitted using equivalent electrical circuits (EEC). The impedance values of electrical components have been iterated to fit experimental impedance data using a fitting software: ZSim-pWin 3.50.

3. Results and discussion

3.1. Curing of the coatings

Curing of the composites was carried out using a standard cycle previously used for the curing of the benzoxazine matrix [6]. The final thickness of all coatings measured by Foucault current (Elcometer 456) was close to 2µm.

In order for polymerization or pre-polymerization to take place, heating is necessary, as the ring opening mechanism is a thermally activated chemical reaction [7]. Fig. 2a shows the FTIR spectra between 370cm^{-1} and 2000cm^{-1} of the P-pPDA coating before and after thermal treatment. Characteristic absorption bands of the oxazine ring appear at 1240cm^{-1} and 1035cm^{-1} (antisymmetric and symmetric stretching of C-O-C respectively) [23,24]. The band at 1365cm^{-1} is attributed to the C-N stretching [25]. Other absorption bands associated with the oxazine ring are observed at 988cm^{-1}, 972cm^{-1} and 937cm^{-1} [26]. After heat treatment, these bands dis-appear in the pristine coating as well as in the borazine **1** containing composites (Fig. 2a and b), which can be attributed to the ring opening mechanism leading to the polymerization of benzoxazine monomer in agreement with previous studies [23,27]. Moreover, a new band is observed at 1674cm^{-1}, which could be attributed to the formation of imine groups by secondary reactions during the curing process [11,28,29]. Finally, the presence of borazine derivative does not appear to modify the FTIR spectra.

The influence of borazine **1** derivative on P-pPDA cross-linking has been investigated for low (0.5 and 3wt%) and higher (10wt%) borazine **1** contents by Differential Scanning Calorimetry.

Using the standard cycle, it has been shown in the literature that the curing degree obtained for the pristine P-pPDA matrix was maximal as no residual enthalpy was observed after a second thermal treatment up to 315°C [9,20]. No clear glass transition temper-ature (T_g) could be determined form DSC data but it is expected to be close to the values reported in the literature for pristine P-pPDA after full curing (i.e. 200°C as measured by DMA) [10] as the evolution of the heat flow signal with temperature did not appear to depend significantly on the composition of the composite.

For the systems containing borazine **1**, DSC results indicate no significant impact of the borazine **1** on the ring-opening polymer-ization of P-pPDA (Fig. 3): both the peak polymerization temperature (T_p) and the polymerization enthalpy (H_R) remain similar for all studied compositions (Table 1).

Thermal curing of the applied coating was further followed up by dielectric analysis (DEA).

A phenomenological approach was adopted to model the dielectric behavior of the chosen benzoxazine during curing.

When free charge migration occurs in a dielectric material, electrical conductivity (σ) as well as dipole polarization contribute to the loss factor ($\varepsilon''(\omega)$)[30]:

(1)

With:

- $\varepsilon''_i = \frac{\sigma}{\omega\varepsilon}$ the ionic polarization contribution, ω the frequency of the electrical field and ε_0 is the dielectric permittivity of vacuum [$\varepsilon_0 = 8854 \cdot 10^{-12}$ AsV^{-1} m^{-1}] [31]
- ε''_d the dipolar polarization contribution (for instance given by the Debye equation in the simple case of a spherical dipole) [30]

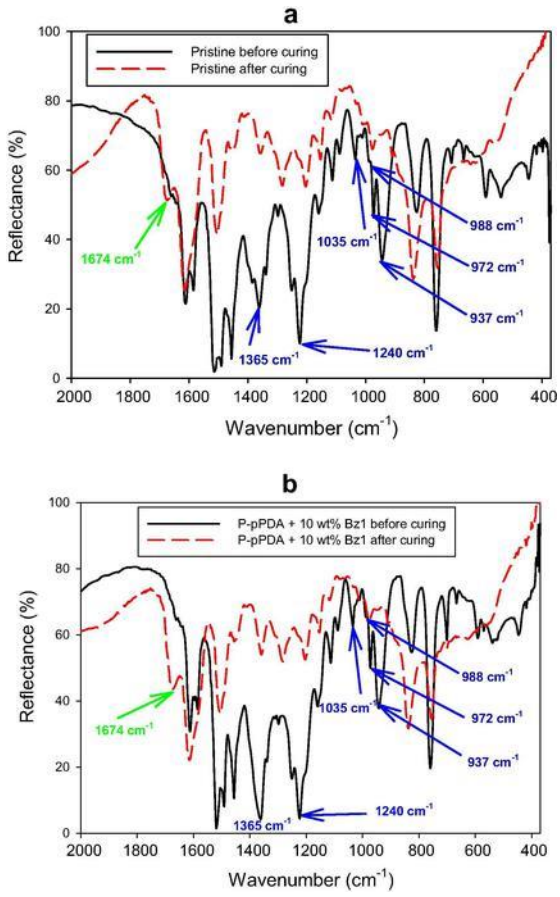

Fig. 2. Comparison of FTIR spectra before and after curing for (a) pristine coatings and (b) P-pPDA+10wt% borazine derivative loaded coatings.

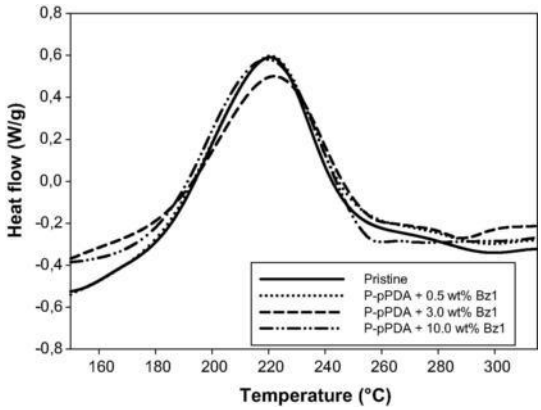

Fig. 3. Differential Scanning Calorimetry performed on P-pPDA formulations with 0, 0.5, 3.0 and 10.0wt% of borazine **1**, respectively.

Table 1
Reaction enthalpy (H_R) and peak polymerization temperature (T_p), during curing of monomers, as determined from DSC data for pristine sample and composites.

Sample	H_R (J/g)	T_p (°C)
Pristine	253	221
P-pPDA+0.5wt% Bz**1**	255	221
P-pPDA+3wt% Bz**1**	249	222
P-pPDA+10wt% Bz**1**	258	220

Of particular interest for curing monitoring is the direct current (DC) conductivity, also known as the inverse ion viscosity, because its relation to a fluid dynamic viscosity (η). This is a measure of the mobility of free ions through a medium under the influence of an electric field.

By its definition, the DC conductivity σ can be expressed as follows:

$\sigma = q\mu n$ (2) where

- q=the charge of free ions [C]
- μ =the free ion mobility [cm^2/Vs]
- n=the free ion concentration [cm^{-3}]

Using also the Einstein and the Stokes-Einstein relations, we obtain a proportionality between 1/σ and η:

$$1/\sigma = \frac{6\pi\eta r}{q^2 n} \quad (3)$$

In Eq. (3), r is the ion radius.

For the interpretation of dielectric spectra (for instance $\varepsilon''(\omega)$), it is important to notice that the ionic current (DC current) can be considered to be almost frequency independent, whereas the energy loss due to reorientation of dipoles varies with frequency.

Under the condition $\varepsilon'' \ll \varepsilon''$, [Eq.1] becomes $\varepsilon'' \approx \frac{\sigma}{\omega\varepsilon}$ and therefore $\log \varepsilon'' \approx \log \sigma - \log \omega$. In that case, an increase of ω with factor 10 leads to a decrease of $log\varepsilon''$ with one unit and this relation has been verified for all systems under study (pristine and composites). Plotting log $\varepsilon''(\log\omega)$ enables then to determine the ionic conductivity from which the viscosity can be determined via Eq. (3).

Fig. 4 shows the change in ion viscosity of the coatings under study with temperature (standard cycle). It appears that the viscosity of pristine benzoxazine and all borazine derivate composites show comparable evolutions with temperature and time, consisting of viscosity decreases during temperature increase steps and viscosity increases related to curing during the isothermal periods, becom-ing superposed at the end of the curing, again supporting the previously observation by DSC in favor of comparable curing degrees at the end of the thermal treatment.

3.2. Textural, physical and chemical analysis of the cured coatings

Coatings with 0, 0.5, 3 and 10wt% of trimesitylborazine **1** have been observed by SEM-FEG and AFM.

SEM-FEG was carried out using Secondary Electron Imaging in topographical mode. Micrographs of coating surfaces in Fig. 5 show that a smooth surface is obtained for the pristine sample and the composite with the lowest borazine **1** content. Starting from

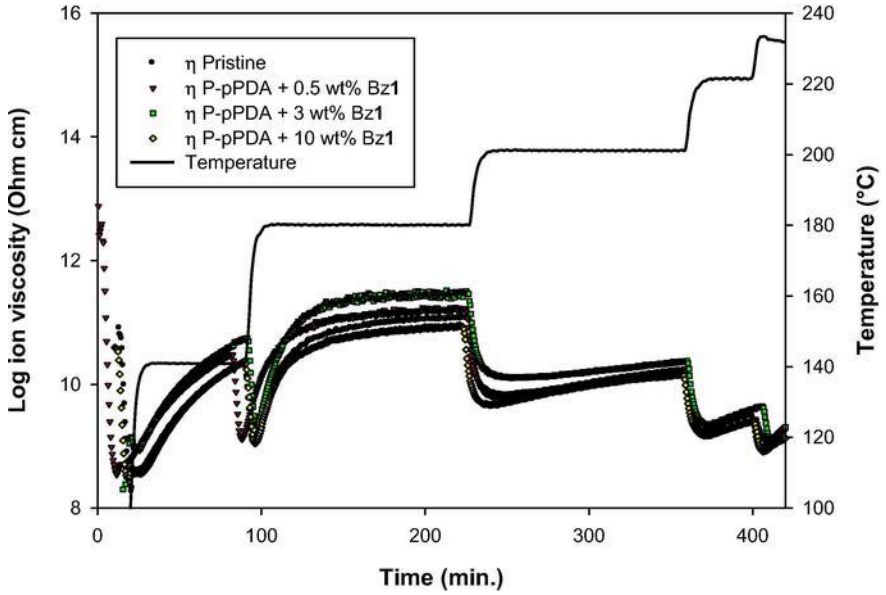

Fig. 4. Evolution of the ion viscosity (η) with temperature for pristine P-pPDA and borazine **1** derivative composites.

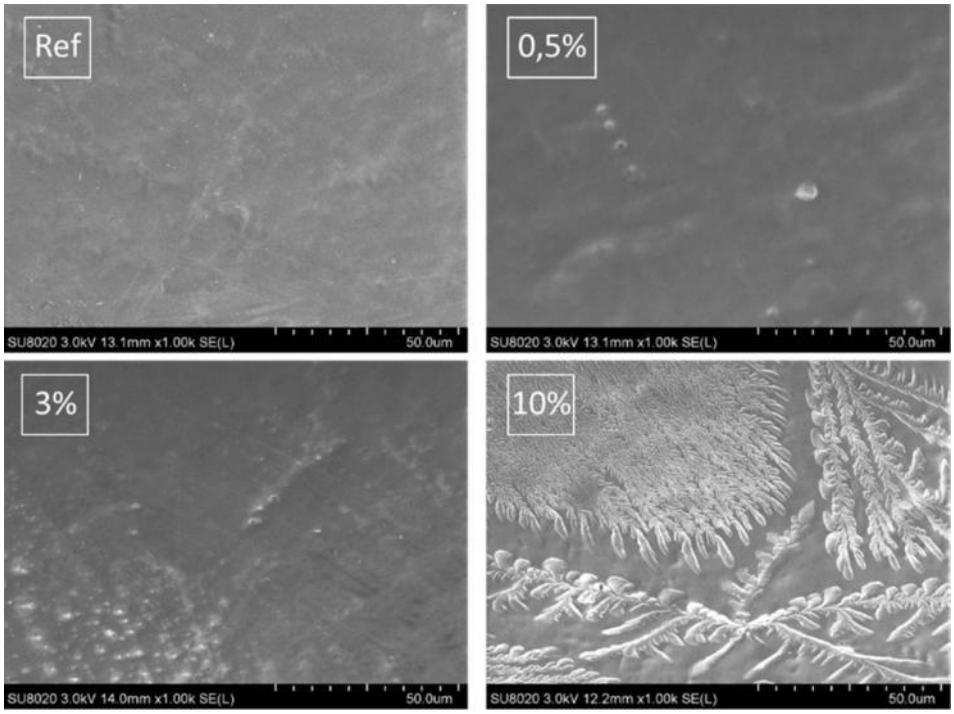

Fig. 5. SEM-FEG images of the surface of coatings containing 0, 0.5, 3 and 10wt% trimesitylborazine **1.**

3wt% borazine **1**, aggregates can be observed, whereas dendritic structures are obtained when 10wt% of trimesitylborazine **1** is incorporated.

In the case of the h-BN epoxy composites studied in the literature, aggregates appear starting from 2wt%, a characteristic for anisotropic structures such as plane orientated conformations. In that case, the low concentration observed for aggregation is not due to any lack of performance in the dispersion process of the anisotropic phase but to a physical phenomenon.

However, one should be careful to use the same interpretation, based on a random distribution between non-interacting particles or molecules within a matrix, for explaining the formation of agglomerates in the case of the borazine derivative composite.

Indeed, it has been shown in the literature [21] that borazine derivative molecules are able to crystalize under certain conditions and therefore, obviously, show a high intermolecular affinity. The formation of clusters of borazine could then be attributed to their crystallization within the P-pPDA matrix, the crystallization enthalpy compensating for the decrease in entropy. If such a crystalline growth process occurs, accompanied by a phase separation, this would mean that the borazine molecules are interacting between them or with the P-pPDA within the composite system and therefore show a fractal behavior as has also been observed in other, ther-moplastic, composites [32–34] where dendritic structures appear very similar to those observed in the 10wt% borazine **1** composite.

Information on the chemical composition of the coating surfaces was, first, gathered together through EDX analysis. The nominal elementary compositions of the benzoxazine monomer and the borazine **1** molecule are shown in Table 2.

EDX analysis carried out on the composite with 10wt% trimesitylborazine **1** is shown in Fig. 6. Two EDX spectra are shown, the first one carried out with the spot focused inside the dendritic structure and, a second one inside the matrix. As can be observed, doing this kind of elementary analysis, the elements present in both spectra are C, O, and N. Some traces of aluminum from the substrate can also be observed. As the EDX analysis has a penetration depth of a couple of microns, the substrate being 2µm thick, this explains why aluminum can also be observed [35]. Moreover, no boron could be detected in either of the spectra. This can be explained by the low sensitivity towards B in EDX analysis and, at the same time, the low B concentration in the borazine **1** molecule

Table 2
Calculated element composition of pristine P-pPDA and composites.

element	Wt% in P-pPDA	Wt% in borazine **1**	Wt% in P-pPDA 0.5 wt% borazine **1**	Wt% in P-pPDA 3.0 wt% borazine **1**	Wt% in P-pPDA 10.0 wt% borazine **1**
H	3.1	6.4	3.1	3.2	3.4
B	0.0	4.9	0.02	0.15	0.5
C	87.8	82.2	87.7	87.6	87.2
O	4.9	0.0	4.9	4.7	4.4
N	4.2	6.4	4.3	4.3	4.5

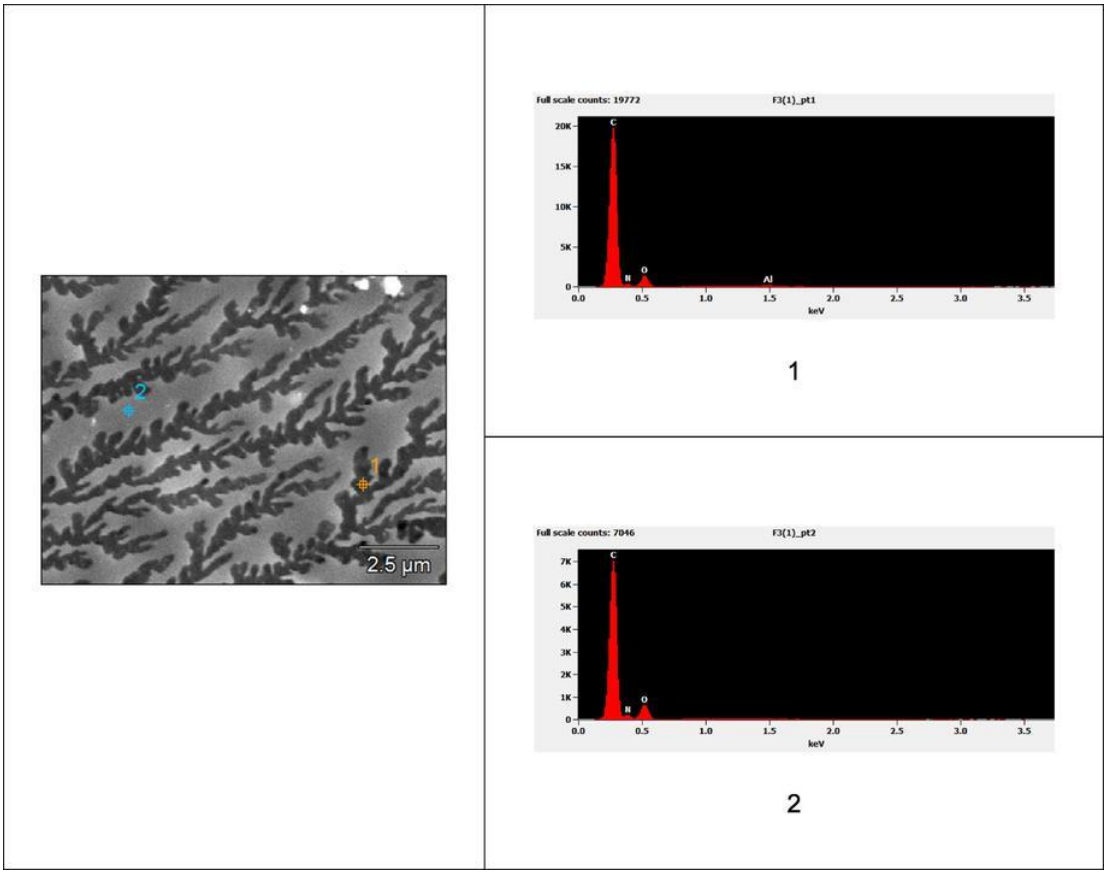

Fig. 6. EDX analyses carried out on dendritic structure (1) and outside this structure (2) for 10wt% borazine **1** composite.

which is 0.5wt% or less and therefore probably below the detection limit of this method. The fact that O can be observed in the matrix as on the dendrite can again be explained by the penetration depth during EDX analysis including, in all cases, the oxygen containing benzoxazine matrix. As a conclusion, Boron appears to be too light and in insufficient proportion to be detected by EDX analysis and there is no significant difference for the other elements (C, O, N) which are, except for O, close in nominal concentration (see Table 2).

The next step in the characterization of the coating has been carried out by AFM analysis. AFM in PeakForce QNM mode was used in order to determine the topography and the roughness of the surface. All samples, from 0 to 3wt% borazine **1**, have relatively low surface roughness, up to 2–5nm, while the sample with 10wt% of borazine **1** has a roughness nearby 40nm (Table 3). The surface RRMS roughness is calculated as the Root Mean Square of a surface measured microscopic peaks and valleys. Final value of surface roughness is an average of values obtained for three different areas probed with different magnification (1, 3 and 10 µm).

In Fig. 7 the surface texture of P-pPDA polymer composites containing different quantities of borazine **1** can be observed. As has also been shown by SEM-FEG analysis, small agglomerates appear starting form 3wt% borazine **1**, whereas dendritic structures appearing in the borazine **1** composite containing 10wt% borazine **1**.

PeakForce QNM mode analysis was further carried out in order to show contrasts appearing in the energy dissipation within the composites. However, as surfaces are not entirely plane – they have no zero roughness – a careful interpretation is needed also con-sidering topographic images. Therefore, PFT images are shown together with topographic images (Fig. 8). Interesting results have been obtained comparing samples with 0.5wt% and 3wt% Bz**1**. As can be observed in Fig. 8a, tiny, well dispersed clusters of a size estimated of about 10–20nm appear in the case of the composite with 0.5wt% borazine derivative. For composites with 3wt% of Bz**1**, clusters with bigger size – around 50–100nm - are also observed. Clustering therefore appears to be inherent to this composite system independent of the concentration of the clustering molecules. This observation is in favor of a phase separation taking place

Table 3
RRMS roughness of pristine cured P-pPDA and composites.

Sample	Pristine	P-pPDA+0.5wt% Bz**1**	P-pPDA+3wt% Bz**1**	P-pPDA+10wt% Bz**1**
RRMS [nm]	4.9	1.1	1.7	37.4

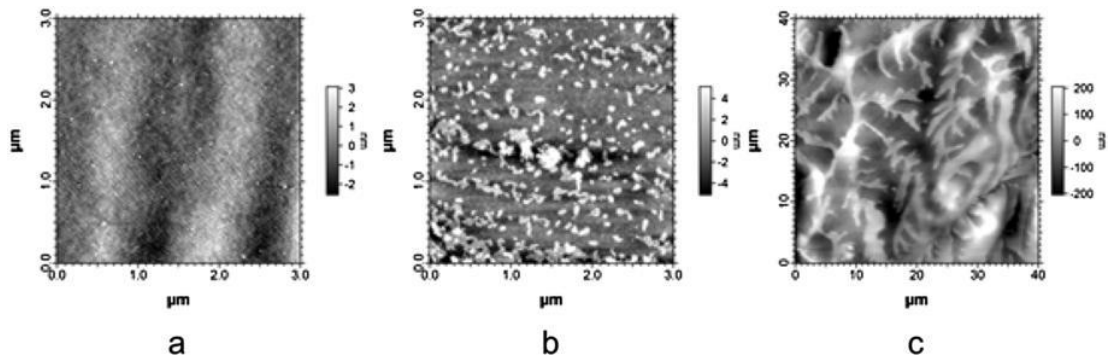

Fig. 7. AFM topography images of borazine **1** derivative containing pPDA polymer composites: (a) polymer pPDA with 0.5wt% of borazine **1** derivative; (b) 3wt% of borazine **1** derivative and (c) 10wt% borazine **1** derivative.

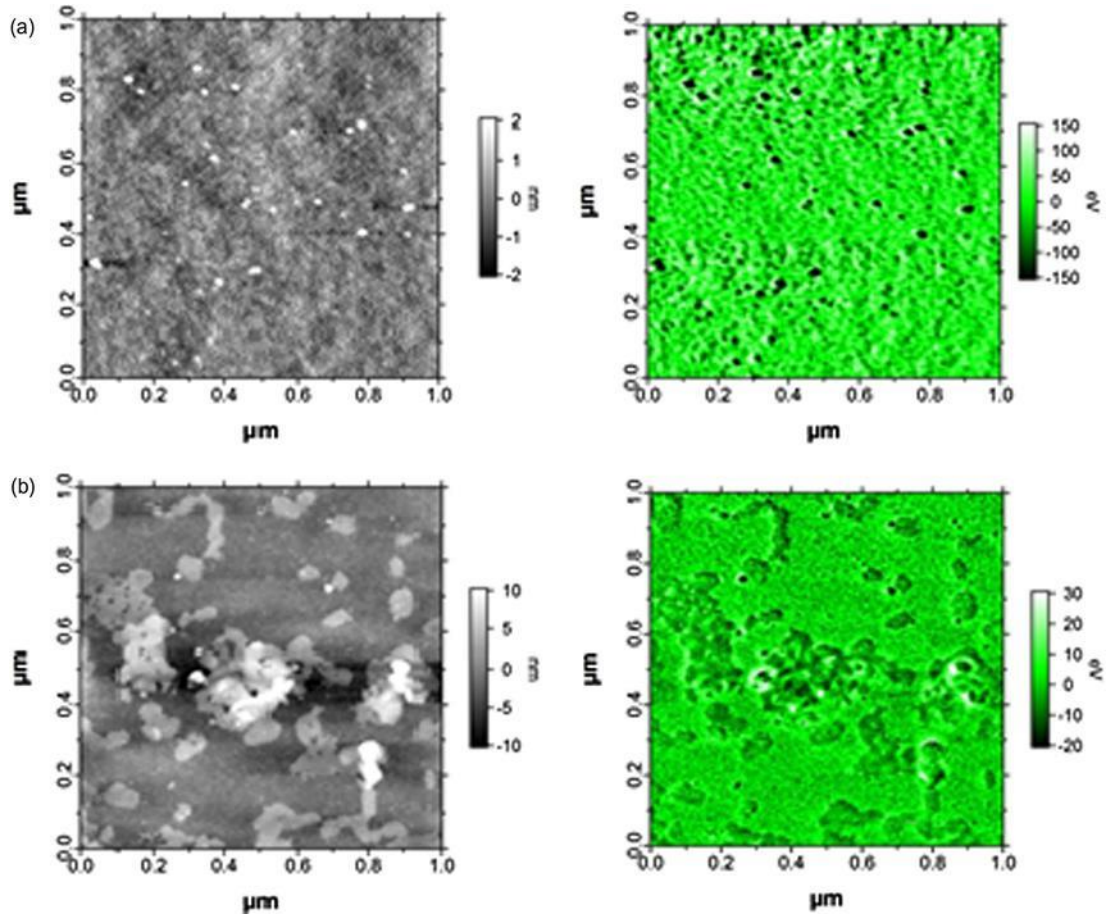

Fig. 8. AFM analysis comparing (a) P-pPDA+0.5wt% Bz **1**. (b) P-pPDA+3wt% Bz **1**. PeakForce QNM – topography in grey, energy dissipation in green. (For interpretation of the references to color in this figure legend, the reader is referred to the web version of this article.)

during the heat treatment of the composite, likely to be related, as mentioned before, to the crystallization induced by the borazine **1** molecules and obviously occurring starting from these low borazine **1** concentrations. At the lowest concentration, the nanometric clusters appear homogeneously dispersed within the matrix, whereas clusters are organized in bigger agglomerates for the higher concentration of borazine derivative. In the last case, the size of the agglomerates appears to be big (100–200nm) with respect to the thickness of the coating (2µm).

Chemical analysis of the coating was further carried out by Tof-SIMS analysis and the intensities of selected molecular fragments were plotted as a function of the sputtering time.

In the borazine **1** composites, borazine derivatives could only be observed in depth in the 10wt% Bz**1** composite as shown in Fig. 9 (after curing) whereas no borazine derivative could be detected in the 0.5wt% and 3wt% sample. Indeed, in the samples with

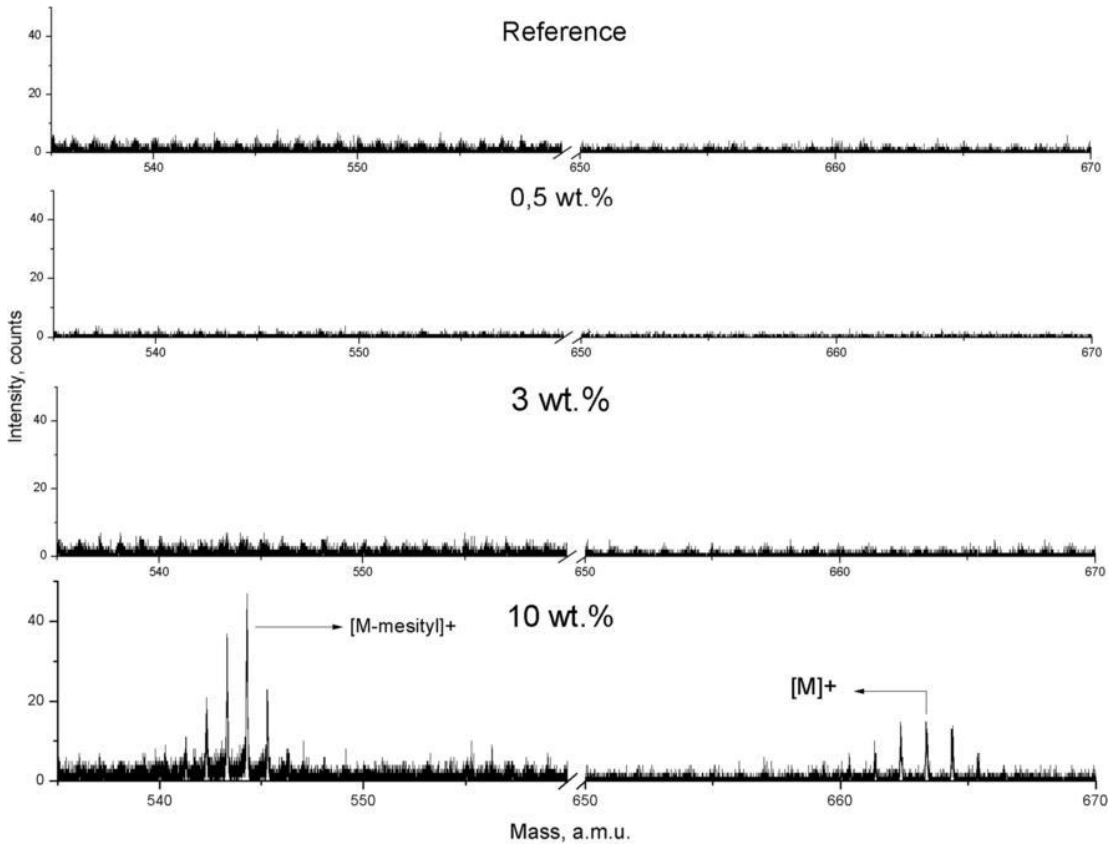

Fig. 9. Comparison of selected mass range in the positive ion mass spectra obtained by SIMS for cured samples with different wt% of borazine **1** derivative and pristine coating measured in the bulk of the coating.

10wt% Bz**1**, completely ionized molecules of $C_{45}H_{48}B_3N_3$ $[M]^{+/-}$ with molecular mass of 663a.m.u. corresponding to the borazine derivative molecule were detected in both polarities. In addition, fragments of the borazine **1** molecule without one mesityl substituent $[M - mesityl]_+$ with molecular mass 544a.m.u. and with additional CH $[M+CH]_+$ (not shown) with molecular mass 676a.m.u. were also found in positive polarity.

Depth profiles of the composites were carried out before and after curing in order to follow the distribution of the borazine **1** related molecules, $[M]_+$ and $[M - mesityl]_+$, whereas $[C_6H_5]_+$ revealed the presence of P-pPDA in the coating. In Fig. 10, we can observe that the intensities of these molecular fragments in the composite with 10wt% Bz**1** are quite uniform after application and drying. After thermal treatment, using the same sputtering conditions, the intensity of the $[C_6H_5]_+$ becomes much lower which is an indicator of the curing of the benzoxazine matrix due to a lower ionization probability. Before and after curing, the $[M]_+$ profile is comparable to the $[M - mesityl]_+$ one but smaller in intensity and the ratio of the borazine **1** related fragments (($[M]_+$)/($[M - mesityl]_+$)) appears to be relatively comparable along the profiles. Therefore, the $[M - mesityl]_+$ fragment is most likely produced upon impact and not damaged during the curing process. Starting from the coating surface, a borazine derivative gradient appears within the P-pPDA benzoxazine matrix, its intensity being much lower at the surface and becoming constant within the bulk of the coating towards the coating/substrate interface. Putting the data of SEM-FEG, AFM and ToF-SIMS profiles together, the interpretation we propose is that the 10wt% borazine derivative composite system shows a dendritic network of borazine derivative as observed by SEM and AFM, buried under a top layer of mainly crosslinked benzoxazine, a couple of hundred nanometers thick. A coverage of the borazine **1** network by benzoxazine could explain both the ToF-SIMS profiles and the small energy dissipation contrast observed in AFM.

Approaching the aluminum substrate, there appears to be a mixed zone where the organic coating and aluminum substrate co-exist and this can be related to the roughness of the aluminum substrate, leading to a region where both coating and substrate are present and sputtered together.

The fact that no borazine derivative is detected in samples with 0.5 or 3wt% borazine derivative can be explained by assuming that a chemical reaction is taking place between the borazine derivative and the P-pPDA. This supports the previous interpretation of the DSC curves (Fig. 2) showing no difference in total enthalpy between pristine P-pPDA and the borazine derivative composites suggesting a contribution of reacting borazine derivative to the total enthalpy.

Finally, the wetting properties of the applied coatings have been compared after determination of the static contact angle. The results are shown in Table 4. The addition of borazine **1** to the P-pPDA matrix appears to increase the static contact angle consider -

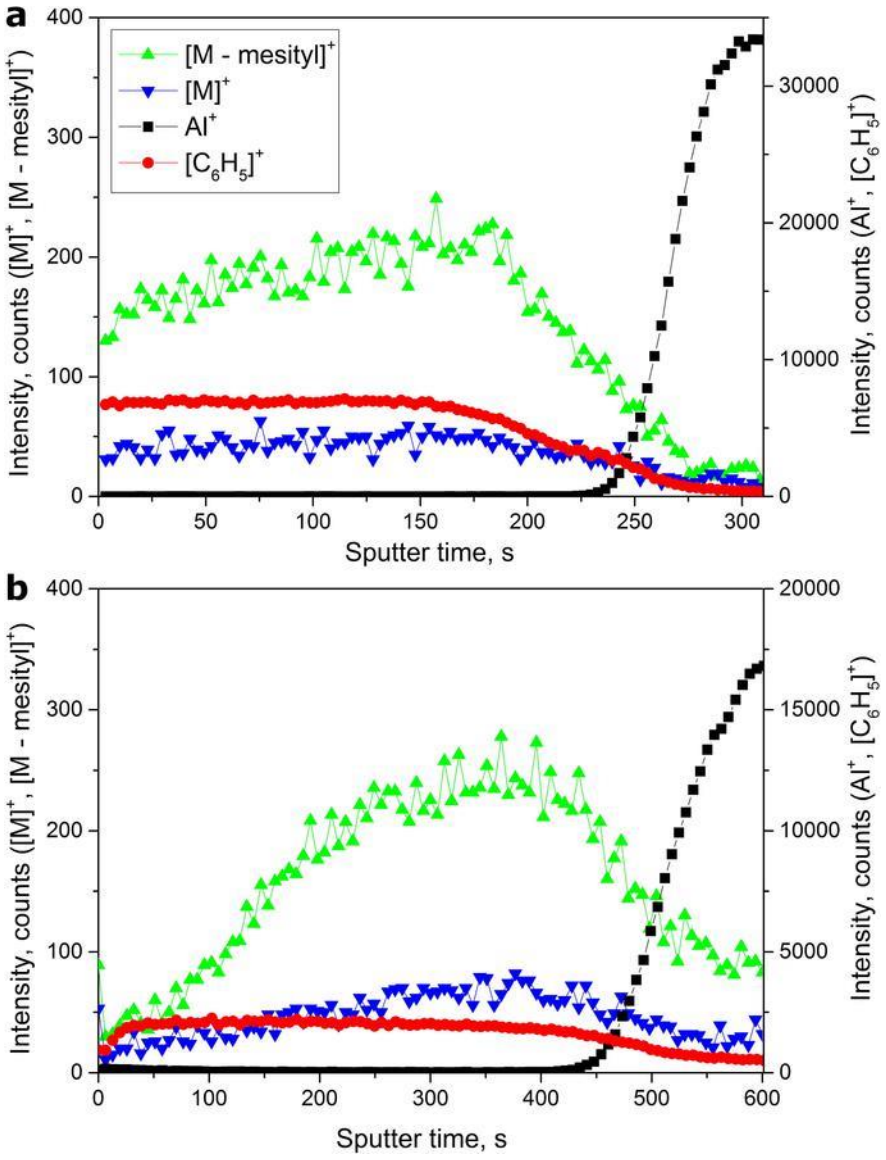

Fig. 10. In depth ToF-SIMS analysis of the quasi-molecular ion (between 661u. and 666u.) and the $[M - mesityl]_+$ (from 541u. to 546u.) in 10wt% Bz**1** coatings before (a) and after curing (b).

Table 4
Evolution of contact angles as a function of borazine concentration.

Sample	Pristine	P-pPDA+0.5wt% Bz**1**	P-pPDA+3wt% Bz**1**	P-pPDA+10wt% Bz**1**
Contact angles (°)	72.5±3.4	96.7±4.4	98.3±2.3	95.4±6.4

ably, highlighting the hydrophobic nature of the added borazine **1**. The decrease in wettability appears to be almost independent of the concentration of borazine **1** or surface roughness of the composite. A priori, the more hydrophobic nature of the composite coating surface, compared to the matrix, is a favorable factor for improving the barrier related corrosion properties of these coatings, as they are potentially retarding or impeding water diffusion through the coating. It should be noticed that the increase in surface roughness (for 10wt% Bz**1**) or higher concentrations of trimesitylborazine did not further increase the contact angle. However, as explained in the electrochemical part (3.3), some defects and/or porosity appear in the coating starting from trimesitylborazine concentrations of 3wt% and higher which are likely to counteract the wetting decrease.

3.3. Electrochemical behavior of P-pPDA borazine composites coated on aluminum and cured with the standard temperature cycle

Coatings on AA1050 have been characterized using Electrochemical Impedance Spectroscopy.

Fig. 11 shows the evolution of Bode plots over immersion time in 0.1M NaCl obtained from EIS on pretreated AA1050, each coated with P-pPDA with concentrations of trimesitylborazine derivative from 0 to 10wt% and cured. At the initial time of immersion, all coatings show a capacitive behavior, with one time constant covering a large range of frequencies and values of the impedance mod-ulus at low frequency (estimation of the resistance of the system) between 10_8 Ω cm_2 for the highest borazine **1** content and almost 10_{10} Ω cm_2 for the 0.5wt% borazine **1** content. Though they display similar barrier properties, a hierarchy between the different for-mulations can be established from the very beginning of the immersion period. Indeed, the presence of 0.5wt% of borazine **1** seems to increase the impedance modulus at low frequency compared to pristine coatings, while higher amounts of borazine **1** appear to decrease this value.

This tendency appears to be confirmed over the whole immersion period. Indeed, after 21days of immersion, the time constants corresponding to the coatings containing borazine **1** contents of 3wt% and higher become narrower and a second time constant appears in the Bode phase plot at lower frequencies, witnessing of the loss of the barrier properties and the presence of a metal/electrolyte interface. Indeed, from concentrations of 3wt% and higher, the barrier properties of P-pPDA borazine **1** composites appear to be even lower than those of a pristine P-pPDA coating after 21days of immersion. As was shown in the SEM-FEG and AFM micrographs, starting from this concentration, agglomerates are formed, which are susceptible to lead to the formation of defects, just as what is observed in the case of 2wt% h-BN epoxy composite in the literature [12]. Consequently, these defects increase the porosity of the coating lowering its barrier properties. Conversely, coatings with 0.5wt% borazine **1** appear to remain highly resistant to corrosion as their properties are maintained after 21days of immersion. Low amounts of borazine **1** (0.5wt%) lead to very durable barrier properties over time when immersed in 0.1M NaCl solution. Corrosion and barrier properties of the coating containing 0.5wt% borazine **1** showing increased stability compared to the pristine P-pPDA coating and even after almost one month of immersion, the

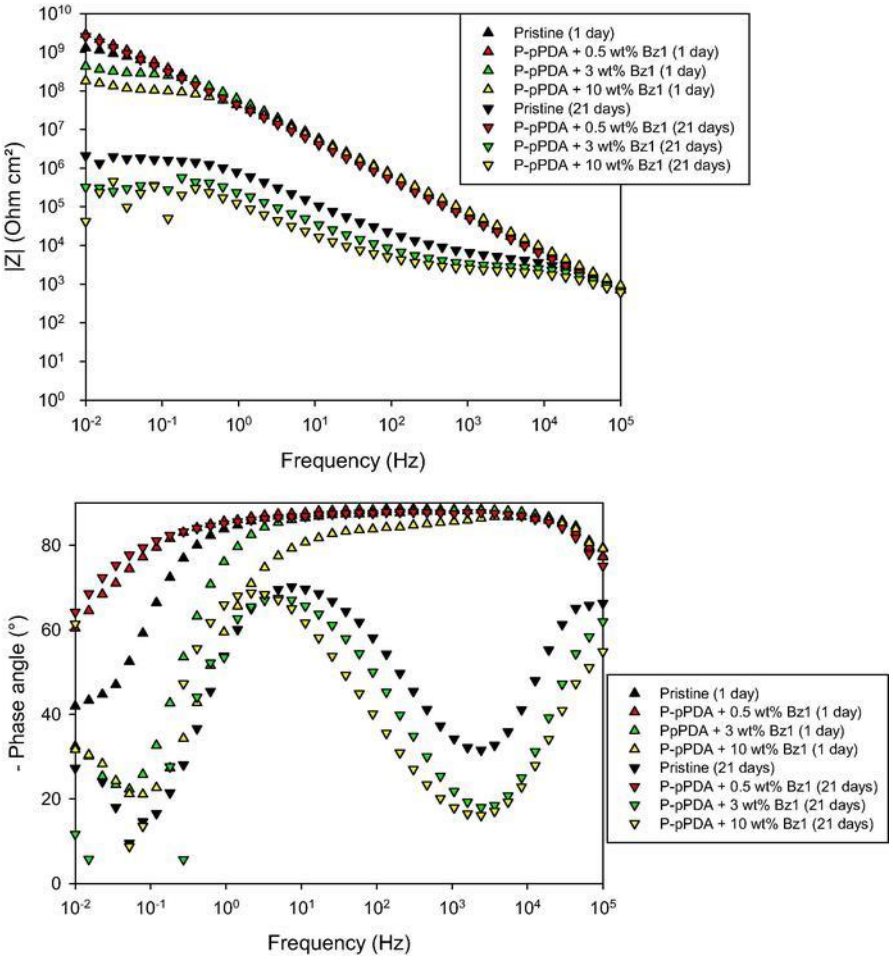

Fig. 11. Bode diagrams of EIS measurements on P-pPDA coatings loaded with different amounts of Bz**1** after one day and 21days of immersion in NaCl 0.1M elec-trolyte.

Bode modulus at low frequency remains of the order of 10^9 Ω cm^2. Moreover, this high time constant still covers a large range of frequencies. It therefore appears that borazine **1** can act as a durable barrier, below a critical concentration. This critical concentration appears to be related to a critical size, as the size of clusters formed are related to this concentration. At a concentration of 0.5wt% of borazine derivative, clusters have sizes of about 10–20nm and are homogeneously dispersed within the matrix, compared to clusters of around 50–100nm for a concentration of 3wt% borazine **1** as well as agglomerates with still bigger sizes which can potentially act as defects. The borazine **1** content in the benzoxazine composite formulation should therefore be kept below a certain threshold to have a positive contribution to the barrier properties.

Impedance data can be fitted using the equivalent electrical circuits presented in Fig. 12, where R_p and Q_c represent the resistance of the pores and the capacitance of the coating respectively. R_{ct} and Q_{dl} are the charge transfer resistance and the double layer capac-itance at the electrolyte/metal interface. R_s represents the resistance of the electrolyte, which is about $1 \cdot 10^2$ Ω cm^2. Constant Phase Elements (CPE) were used instead of pure capacitances in order to take into account the non-ideal behavior of the organic layer and the electrochemical double layer. In the literature, the impedance of a constant phase element is written as $Z = 1/(i\omega)^n Q$ where Q is the CPE parameter equal to the admittance at ω =1rads^{-1} and n is the frequency dispersion factor varying from 0 to 1. If n=0, the CPE behaves as a resistor. If n=1, the CPE is a pure capacitance [36]. In this case, n is higher than 0.9, reflecting a very capacitive behavior.

Fig. 13 compares the time evolution of the calculated pores resistance R_p for coatings applied on bare pretreated AA1050 as a function of the borazine **1** content. In the very first times of immersion, all coatings exhibit R_p values higher than 10^9 Ω cm^2 and are best fitted by the equivalent circuit a. Coatings with 0.5wt% of borazine **1** maintain very high R_p values up to 47days of immersion in the saline solution. A low amount of borazine **1** (0.5wt%) appears to significantly improve the pores resistance of the P-pPDA coatings and this can be related to the corresponding microstructure. Indeed, clusters having sizes of about 10–20nm form a dense homogeneously dispersed barrier, impeding or limiting water penetration and avoiding the propagation of cracks through the coating and can therefore be represented by the EEC model a.

However, for higher borazine **1** amounts, in the first days of immersion, a faster decrease in R_p values is observed, compared to pristine coatings which could be explained by the formation of preferential pathways for aggressive species through the organic layer, related to the agglomerates or dendritic structures formed within the matrix. Consequently, water from the outside can penetrate though the coating and reach the metal/coating interface, which is represented by the EEC model b.

Pristine coatings and 3wt% and 10wt% Bz**1** loaded coatings exhibit R_p values as low as 10^3–10^4 Ω cm^2 after 21days of immersion and are all best fitted by the equivalent circuit b. Therefore, though the borazine **1** composites all have increased hydrophobic prop-erties, this is not translated by an increase of the corrosion resistance for concentrations equal or above 3wt% of Bz**1**.

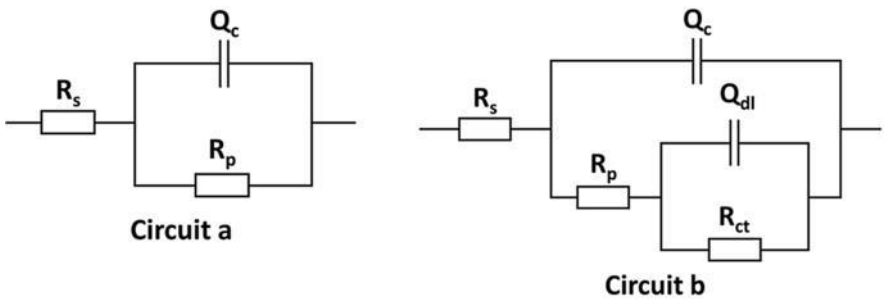

Fig. 12. Equivalent electrical circuits used to fit impedance data.

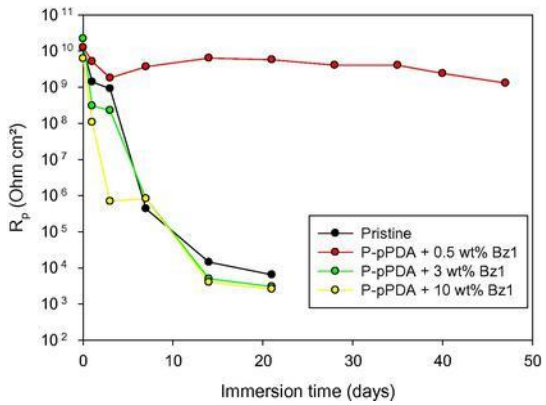

Fig. 13. Evolution over immersion time in 0.1M NaCl of the calculated pore resistance R_p value for P-pPDA coatings with different amounts of borazine **1.**

4. Conclusions

A composite coating, 2µm in thickness, consisting of a benzoxazine matrix (P-pPDA) mixed with B-Trimesytil-N-triphenylborazine in different concentrations – ranging from 0.5wt% up to 10wt% – has been applied on an aluminum substrate by spin coating followed by curing at high temperature (up to 230°C).

The curing degree of the benzoxazine matrix appeared to be highly completed, comparable to the pristine benzoxazine and did not appear to be influenced by the presence of the borazine derivative as shown by FTIR, DSC and DEA analyses.

Addition of the borazine derivative rendered the coating more hydrophobic compared to the pristine benzoxazine coating. Af-ter application and drying, the borazine derivative showed a homogeneous concentration profile as shown by ToF-SIMS analysis. However, after curing, close to the surface of the coating, a concentration gradient was observed towards the surface of the coating for the composite with 10wt% borazine derivative. No borazine derivative is detected by ToF-SIMS in samples with 0.5 or 3wt% borazine derivative indicating that a chemical reaction is taking place between the borazine derivative and the P-pPDA. Moreover, the microstructure sensibly depended on the borazine derivative content. Indeed, for concentrations as low as 0.5wt% of borazine derivative, a nanocomposite structure was obtained, with nanoclusters 10–20nm in size, with the secondary phase homogeneously dispersed through the matrix. For higher concentrations, first, an agglomerated microstructure was obtained for 3wt% of borazine derivative content, whereas for the highest concentration (10wt% of borazine derivative) dendritic structures appeared.

The corrosion properties of the synthesized composites, strongly depend on their microstructure. At 0.5wt% borazine derivative, the barrier properties having a homogeneous nanocomposite structure appeared to be highly improved and more durable with respect to the pristine benzoxazine. Conversely, for higher concentrations, starting from 3wt%, the formation of agglomerates or dendritic structures for the highest concentration decreased the barrier properties, suggesting the presence of flaws in these materials translated by easier water percolation through the sample down to the metal-coating interface.

It therefore appears that the synthesized borazine derivative can act as a durable corrosion barrier, below a critical concentration related to the size of the secondary phase generated within the composite.

5. Data availability

The raw/processed data required to reproduce these findings cannot be shared at this time due to time limitations.

Conflicts of interest

There are no conflicts of interest.

Acknowledgments

The authors also want to thank the ‘‘Région Wallonne’’ in the framework of the Programme d’Excellence “FLYCOAT”, the FEDER 2014-2020 program (“HYBRITIMESURF”, “MACOBIO” projects) and the Interreg V program (“BIOCOMPAL” project). The authors wish to thank SONACA for particularly endorsing this part of the Flycoat project. Finally, the authors wish to thank Mrs Amandine Portier for her specific contribution in preparing and characterizing the samples at the Department of Material Science of the Univer-sity of Mons.

Appendix A. Supplementary material

Supplementary data to this article can be found online at https://doi.org/10.1016/j.eurpolymj.2018.10.018.

References

[1] A. Foyet, T.H. Wu, A. Kodentsov, L.G. Van der Ven, G. De With, R.A. Van Benthem, Absorption of water and corrosion performance of a clear and pigmented epoxy coating on Al-2024 Alloy, in: ECS Trans. 25 (Issue 29) Coatings Corros. Prot., 2010, pp. 31–39. doi:10.1149/1.3327222.

[2] S. Sharifi Golru, M.M. Attar, B. Ramezanzadeh, Effects of different surface cleaning procedures on the superficial morphology and the adhesive strength of epoxy coating on aluminium alloy 1050, Prog. Org. Coat. 87 (2015) 52–60, https://doi.org/10.1016/j.porgcoat.2015.05.005.

[3] H. Ishida, D.J. Allen, Physical and mechanical characterization of near-zero shrinkage polybenzoxazines, J. Polym. Sci. Part B Polym. Phys. 34 (1996) 1019–1030, https://doi.org/10.1002/(SICI)1099-0488(19960430)34:6<1019::AID-POLB1>3.0.CO;2-T.

[4] H.-C. Liu, W.-C. Su, Y.-L. Liu, Self-assembled benzoxazine-bridged polysilsesquioxanes exhibiting ultralow-dielectric constants and yellow-light photolumines-cent emission, J. Mater. Chem. 21 (2011) 7182, https://doi.org/10.1039/c1jm10815h.

[5] J. Escobar, M. Poorteman, L. Dumas, L. Bonnaud, P. Dubois, M.-G. Olivier, Thermal curing study of bisphenol A benzoxazine for barrier coating applications on 1050 aluminum alloy, Prog. Org. Coat. 79 (2015) 53–61, https://doi.org/10.1016/j.porgcoat.2014.11.004.

[6] M. Poorteman, A. Renaud, J. Escobar, L. Dumas, L. Bonnaud, P. Dubois, M. Olivier, Thermal curing of para -phenylenediamine benzoxazine for barrier coating applications on 1050 aluminum alloys, Prog. Org. Coat. 97 (2016) 99–109, https://doi.org/10.1016/j.porgcoat.2016.03.026.

[7] H. Ishida, Y. Rodriguez, Curing kinetics of a new benzoxazine-based phenolic resin by differential scanning calorimetry, Polymer 36 (1995) 3151–3158, https: //doi.org/10.1016/0032-3861(95)97878-J.

[8] N.N. Ghosh, B. Kiskan, Y. Yagci, Polybenzoxazines-New high performance thermosetting resins: synthesis and properties, Prog. Polym. Sci. 32 (2007) 1344–1391, https://doi.org/10.1016/j.progpolymsci.2007.07.002.

[9] L. Dumas, L. Bonnaud, M. Olivier, M. Poorteman, P. Dubois, Facile preparation of a novel high performance benzoxazine–CNT based nano-hybrid network ex-hibiting outstanding thermo-mechanical properties, Chem. Commun. 49 (2013) 9543, https://doi.org/10.1039/c3cc45179h.

[10] L. Dumas, L. Bonnaud, M. Olivier, M. Poorteman, P. Dubois, High performance benzoxazine/CNT nanohybrid network – An easy and scalable way to combine attractive properties, Eur. Polym. J. 58 (2014) 218–225, https://doi.org/10.1016/j.eurpolymj.2014.06.023.
[11] H. Oie, A. Sudo, T. Endo, Acceleration effect of N-allyl group on thermally induced ring-opening polymerization of 1,3-benzoxazine, J. Polym. Sci. Part A Polym. Chem. 48 (2010) 5357–5363, https://doi.org/10.1002/pola.24338.
[12] M. Cui, S. Ren, S. Qin, Q. Xue, H. Zhao, L. Wang, Non-covalent functionalized hexagonal boron nitride nanoplatelets to improve corrosion and wear resistance of epoxy coatings, RSC Adv. 7 (2017) 44043–44053, https://doi.org/10.1039/C7RA06835B.
[13] M. Cui, S. Ren, S. Qin, Q. Xue, H. Zhao, L. Wang, Processable poly(2-butylaniline)/hexagonal boron nitride nanohybrids for synergetic anticorrosive reinforce-ment of epoxy coating, Corros. Sci. 131 (2018) 187–198, https://doi.org/10.1016/j.corsci.2017.11.022.
[14] I. Balberg, C.H. Anderson, S. Alexander, N. Wagner, Excluded volume and its relation to the onset of percolation, Phys. Rev. B. 30 (1984) 3933–3943, https:// doi.org/10.1103/PhysRevB.30.3933.
[15] Y.H. Wang, C.M. Chang, Y.L. Liu, Benzoxazine-functionalized multi-walled carbon nanotubes for preparation of electrically-conductive polybenzoxazines, Poly-mer 53 (2012) 106–112, https://doi.org/10.1016/j.polymer.2011.11.040.
[16] C. Zúñiga, L. Bonnaud, G. Lligadas, J.C. Ronda, M. Galià, V. Cádiz, P. Dubois, Convenient and solventless preparation of pure carbon nanotube/polybenzox-azine nanocomposites with low percolation threshold and improved thermal and fire properties, J. Mater. Chem. A. 2 (2014) 6814–6822, https://doi.org/10. 1039/C4TA00217B.
[17] L. Dumas, L. Bonnaud, P. Dubois, Polybenzoxazine nanocomposites, In: Adv. Emerg. Polybenzoxazine Sci. Technol., Elsevier, 2017, pp. 767–800, https://doi. org/10.1016/B978-0-12-804170-3.00038-X.
[18] L. Shen, Y. Zhao, Y. Wang, R. Song, Q. Yao, S. Chen, Y. Chai, A long-term corrosion barrier with an insulating boron nitride monolayer, J. Mater. Chem. A. 4 (2016) 5044–5050, https://doi.org/10.1039/C6TA01604A.
[19] S. Saiev, L. Bonnaud, P. Dubois, D. Beljonne, R. Lazzaroni, Modeling the formation and thermomechanical properties of polybenzoxazine thermosets, Polym. Chem. 8 (2017) 5988–5999, https://doi.org/10.1039/C7PY00995J.
[20] A. Renaud, M. Poorteman, J. Escobar, L. Dumas, Y. Paint, L. Bonnaud, P. Dubois, M.G. Olivier, A new corrosion protection approach for aeronautical applica-tions combining a Phenol-paraPhenyleneDiAmine benzoxazine resin applied on sulfo-tartaric anodized aluminum, Prog. Org. Coat. 112 (2017) 278–287, https: //doi.org/10.1016/j.porgcoat.2017.07.007.
[21] S. Kervyn, O. Fenwick, F. Di Stasio, Y.S. Shin, J. Wouters, G. Accorsi, S. Osella, D. Beljonne, F. Cacialli, D. Bonifazi, Polymorphism, fluorescence, and optoelec-tronic properties of a borazine derivative, Chem. – A Eur. J. 19 (2013) 7771–7779, https://doi.org/10.1002/chem.201204598.
[22] S.J. Groszos, S.F. Stafiej, Organoboron compounds. I. A new synthesis of B-Trialkyl and Triaryl-N-triphenylborazoles 1, J. Am. Chem. Soc. 80 (1958) 1357–1360, https://doi.org/10.1021/ja01539a021.
[23] P. Lorjai, S. Wongkasemjit, T. Chaisuwan, A.M. Jamieson, Significant enhancement of thermal stability in the non-oxidative thermal degradation of bisphe-nol-A/aniline based polybenzoxazine aerogel, Polym. Degrad. Stab. 96 (2011) 708–718, https://doi.org/10.1016/j.polymdegradstab.2010.12.005.
[24] T. Agag, T. Takeichi, Synthesis and characterization of novel benzoxazine monomers containing allyl groups and their high performance thermosets, Macromol-ecules. 36 (2003) 6010–6017, https://doi.org/10.1021/ma021775q.
[25] S. Ren, X. Yang, X. Zhao, Y. Zhang, W. Huang, An m -phenylenediamine-based benzoxazine with favorable processability and its high-performance thermoset, J. Appl. Polym. Sci. 133 (2016) https://doi.org/10.1002/app.43368
[26] S. Nalakathu Kolanadiyil, M. Azechi, T. Endo, Synthesis of novel tri-benzoxazine and effect of phenolic nucleophiles on its ring-opening polymerization, J. Polym. Sci. Part A Polym. Chem. 54 (2016) 2811–2819, https://doi.org/10.1002/pola.28167
[27] T. Takeichi, Y. Guo, S. Rimdusit, Performance improvement of polybenzoxazine by alloying with polyimide: effect of preparation method on the properties, Polymer 46 (2005) 4909–4916, https://doi.org/10.1016/j.polymer.2005.03.096.
[28] S. Ren, X. Yang, X. Zhao, Y. Zhang, W. Huang, Synthesis, characterization, and polymerization of a novel benzoxazine based on diethyltoluenediamine, J. Appl. Polym. Sci. 132 (2015) https://doi.org/10.1002/app.41920
[29] A. Sudo, L.-C. Du, S. Hirayama, T. Endo, Substituent effects of N-alkyl groups on thermally induced polymerization behavior of 1,3-benzoxazines, J. Polym. Sci. Part A Polym. Chem. 48 (2010) 2777–2782, https://doi.org/10.1002/pola.24026.
[30] F. Kremer, A. Schönhals (Eds.), Broadband Dielectric Spectroscopy, Springer, Berlin, Heidelberg, 2003https://doi.org/10.1007/978-3-642-56120-7.
[31] C. Liu, D. Shen, R.M. Sebastián, J. Marquet, R. Schönfeld, Mechanistic studies on ring-opening polymerization of benzoxazines: a mechanistically based catalyst design, Macromolecules. 44 (2011) 4616–4622, https://doi.org/10.1021/ma2007893.
[32] L. Gránásy, T. Pusztai, T. Börzsönyi, J.A. Warren, J.F. Douglas, A general mechanism of polycrystalline growth, Nat. Mater. 3 (2004) 645–650, https://doi.org/ 10.1038/nmat1190.
[33] V. Ferreiro, J.F. Douglas, J.A. Warren, A. Karim, Nonequilibrium pattern formation in the crystallization of polymer blend films, Phys. Rev. E. 65 (2002) 42802, https://doi.org/10.1103/PhysRevE.65.042802.
[34] B.C. Okerberg, H. Marand, J.F. Douglas, Dendritic crystallization in thin films of PEO/PMMA blends: a comparison to crystallization in small molecule liquids, Polymer 49 (2008) 579–587, https://doi.org/10.1016/j.polymer.2007.11.034.
[35] J.R.M. Joseph Goldstein, Dale E. Newbury, David C. Joy, Charles E. Lyman, Patrick Echlin, Eric Lifshin, Linda C. Sawyer (Eds.), Scanning Electron Microscopy and X-Ray Microanalysis, Kluwer Aca, 2003https://doi.org/10.1016/j.micron.2003.08.001.
[36] P. Zoltowski, On the electrical capacitance of interfaces exhibiting constant phase element behaviour, J. Electroanal. Chem. 443 (1998) 149–154, https://doi. org/10.1016/S0022-0728(97)00490-7.